Inhibition of Tumor Growth Progression by Antiandrogens and mTOR Inhibitor in a *Pten*-Deficient Mouse Model of Prostate Cancer

Weisheng Zhang,[1] Joe Zhu,[1] Clay L. Efferson,[2] Chris Ware,[3] Jennifer Tammam,[2] Minilik Angagaw,[4] Jason Laskey,[2] Kimberly A. Bettano,[1] Shailaja Kasibhatla,[2] John F. Reilly,[3] Cyrille Sur,[5] and Pradip K. Majumder[2]

Departments of [1]Imaging, [2]Oncology, [3]Pharmacology, and [4]Laboratory Animal Research, Merck Research Laboratories, Boston, Massachusetts; and [5]Imaging Department, Merck Research Laboratories, West Point, Pennsylvania

Abstract

Androgen receptors have been shown to play a critical role in prostate cancer. We used ultrasound imaging techniques to track tumor response to antiandrogen and rapamycin treatment in a prostate-specific Pten-deleted mouse model of cancer. Depletion of androgens by either surgical or chemical castration significantly inhibited tumor growth progression without altering the activation of Akt and mammalian target of rapamycin (mTOR). We also showed for the first time that targeting mTOR along with antiandrogen treatment exhibited additive antitumor effects *in vivo* when compared with single agents. Our preclinical data suggest that combination of antiandrogens with mTOR inhibitors might be more effective in treating androgen-dependent prostate cancer patients. [Cancer Res 2009;69(18):7466–72]

Introduction

The prevalence of prostate cancer is particularly high in developed countries and is the third most common cause of cancer-related deaths in men. Prevalence is now also increasing in developing nations (1). It was predicted by the American Cancer Society that in the United States alone, ~192,280 men would be diagnosed with prostate cancer and 27,360 deaths would be attributed to prostate cancer this year. Prostate cancer is the second most frequently diagnosed cancer in men in the United States with more than two million currently suffering from this disease. Although the death rate from prostate cancer is decreasing with the advent of early diagnosis, it still remains a leading cause of cancer-related death in men. Currently available treatment modalities include radical prostectomy, chemotherapy, radiotherapy, and androgen ablation therapy.

The sex hormone testosterone plays a central role in the normal development and growth of male sex organs, as well as the abnormal growth of prostate cancer, through the androgen receptor (AR) signaling pathway (reviewed in ref. 2). Although the mechanism of androgen dependence in prostate tumor growth is not fully understood, the primary goal of treatment for prostate cancer in the clinic is to achieve suppression or inhibition of AR activation by androgen deprivation through surgical castration, estrogen, antiandrogens, or their combination (reviewed in ref. 3). Androgen ablation by either surgical castration or by luteinizing hormone–releasing hormone analogue strongly inhibits the growth of localized advanced cancer by eliminating circulating testosterone (4, 5). However, within only a few years after androgen ablation therapy, prostate cancer growth in these patients tends to become more aggressive as well as androgen-independent (reviewed in ref. 6). The mechanism of developed resistance to antiandrogens remains unclear, yet cell-based studies indicate that regulation of the phosphoinositide 3-kinase (PI3K) pathway by androgens may play a critical role in the development of androgen independent prostate cancer (7–9).

The PI3K pathway plays an important role in regulating several cellular functions including cell growth, proliferation, differentiation, and survival. Loss or functional alteration of the tumor suppressor gene *PTEN* activates downstream PI3K signaling, resulting in increased cell proliferation and survival (10–14). More than 20% of primary human prostate cancer is associated with deletion or functional loss of *PTEN*, whereas >50% of human metastatic prostate cancer specimens harbor biallelic loss of this gene, suggesting that PTEN might be responsible for the lethal form of the disease (15–24). Conventional deletion of both alleles of *Pten* leads to embryonic lethality (25, 26), whereas heterozygous *Pten*-null mice develop prostate intraepithelial neoplasia or PIN. These mice have been crossed with a number of other genetically engineered mice for further enhancement of the tumor phenotype [reviewed in Majumder and colleagues (27)]. Loss of function mutations or lowered expression of *PTEN* increases the activity of important downstream targets of PI3K such as AKT in various cell lines and engineered mouse models (reviewed in refs. 28, 29). Activation of *AKT1* in the prostate alone induces development of PIN but not invasive prostate cancer, whereas activation of *AKT1* in a $p27^{Kip1}$ null setting as well as prostate-specific deletion of *Pten* induces invasive cancer in mice (30–32). To understand the role of androgen ablation in the context of PI3K pathway activation, we have used a genetically engineered mouse model where $Pten^{loxP/loxP}$ mice (33) were crossed with ARR2-Pb-Cre^{+} transgenic mice (34). These mice spontaneously develop prostate tumors that recapitulate most human prostate cancer characteristics (32). However, selection and enrollment of these animals into a preclinical study are difficult due to the fact that the anatomic location of these tumors prohibits standard caliper measurements. Therefore, monitoring the kinetics of tumor response to a therapy in live animals is challenging. Here, we evaluated the use of the translational three-dimension ultrasound

Note: Supplementary data for this article are available at Cancer Research Online (http://cancerres.aacrjournals.org/).

J. Zhu, C. Efferson, and C. Ware contributed equally.

Requests for reprints: Weisheng Zhang, Imaging Department, Merck Research Laboratories, 33 Avenue Louis Pasteur, Boston, MA 02115. Phone: 617-992-3061; Fax: 617-992-2487; E-mail: weisheng_zhang@merck.com and Pradip K. Majumder, Department of Oncology, Merck Research Laboratories, 33 Avenue Louis Pasteur, Boston, MA 02115. Phone: 617-992-2281; Fax: 617-992-2486; E-mail: pradip_majumder@merck.com.

doi:10.1158/0008-5472.CAN-08-4385

imaging technology to visualize and follow tumor development and response to androgen deprivation treatments. We show that this model is androgen dependent and that androgen blockade does not affect the activation of Akt or mammalian target of rapamycin (mTOR). We also show that simultaneous inhibition of mTOR and androgen signaling induces better antitumor effect in this model.

Materials and Methods

Animals. A conditional Pten-deficient model of prostate cancer (*Pten*$^{loxp/loxp}$/Pb-Cre4) in which *Pten* is homozygously deleted in the prostate gland due to prostate-specific expression of Cre recombinase (32) was used for these studies. This model was obtained from Dr. Hong Wu's laboratory at the University of California in Los Angles, CA. Both founder lines, the ARR2Probasin-Cre (C+) transgenic mice (on C57BL/6xDBA2 background; ref. 34) and the *Pten*$^{Loxp/Loxp}$ mice (on a 129/BALB/c background), were maintained in our contract facility. The heterozygous *Pten*$^{Loxp/+}$;C/+ males were then bred to *Pten*$^{Loxp/Loxp}$ females to obtain the *Pten*$^{Loxp/loxp}$;C/+ genotype. Male *Pten*$^{Loxp/loxp}$;C/+ mice between 14 and 76 wk of age were used for experiments. Mice were using an isolated barrier unit system on wood-chip bedding and fed standard rodent chow *ad libitum*. All animal procedures were reviewed and approved by the Merck Research Laboratories-Boston Institutional Animal Care and Use Committee.

3-Dimensional ultrasound imaging of prostate tumors. Mice were anaesthetized with a continuous flow of 2% to 3% isoflurane in oxygen mixture (2.5 liters/min) in an induction chamber using the Vevo anesthesia system (VisualSonics, Inc.). Mice were placed on the Vevo Mouse Handling Table (37°C) in the Vevo Integrated Rail System (VisualSonics, Inc.) with continuous isoflurane anesthesia. Mouse fur was removed before ultrasound imaging. Ultrasound coupling gel AQUASONIC 100 (Parker Laboratories, Inc.) was applied directly to the skin. Mice were then scanned transversely from ventral body wall using the 710B real-time microvisualization scanhead (probe) and Vevo770 High-resolution *In vivo* Micro-Imaging system (VisualSonics, Inc.). The 710B scanhead provides a center frequency at 20 MHz with 70 μm axial and 140 μm lateral resolution at the focal depth of 15 mm. The stepsize of scanning varies from 32 to 48 μm dependent on the scanning distance. The maximal field of view of the scanhead is 20.8 × 20.8 mm and the maximal scanning distance is 24 mm. Animals were scanned twice due to tumor growth in both anterior lobes of the prostate. A single scan was insufficient to cover both tumors in the same field of view. Three-dimensional images were reconstructed from two-dimensional section images using the Vevo770 system software following acquisition. Tumor volumes were determined using the three-dimensional Quantify Version 3.5 software (Robarts Research Institute).

Animal surgery and treatment. Animals were prescreened by ultrasound three-dimensional imaging to obtain a baseline tumor volume for enrollment and were randomized into groups based on tumor volumes. For studies using androgen ablation by surgical castration, 20 animals with tumors 324 to 739 mm^3 were randomized into two groups. Ten animals were castrated by removal of both testicles following the standard operation procedure of Merck Institutional Animal Care and Use Committee protocols. The other 10 animals were kept as controls. Mice were imaged weekly. Nine weeks following castration, slow-releasing testosterone propionate pellets (100 mg of 90-day-releasing pellet purchased from Innovative Research of America) were implanted s.c. and ultrasound imaging resumed after a period of 2 wk. Testosterone pellets were then removed 5 wk following implantation and tumor kinetics were tracked for an additional 5 wk. Chemical castration studies were conducted with Casodex at the dose of 10 mg/kg, daily for 5 d a week (Monday to Friday). Tumor-bearing mice were also treated with Rapamycin (LC Laboratories) alone at the dose of 20 mg/kg, daily (Monday to Friday), or with the combination of Casodex + Rapamycin at their above indicated doses, daily (Monday to Friday) or by 0.5% methyl cellulose (as vehicle) for 8 wk. Mice were imaged weekly throughout treatment. BrdUrd (Roche) was administered i.p. at a dose of 50 mg/kg. Mice were euthanized and tumors were dissected, weighed, and processed for further analysis at the conclusion of studies.

End point tumor assessment. Mice were euthanized using CO_2 and entire tumors were collected and weighed. Due to the variable amount of fluid that the tumors in this model contain, net tumor weight was also measured after fluid removal. Animals were euthanized and tumor samples were collected when tumor volumes reached 10% of body weight or tumor size was out of range of the ultrasound transducer before study termination. Tumor samples were collected for histologic and biochemical analysis.

Plasma concentration of testosterone. Mice were euthanized using CO_2 and 500 μL of blood was collected by cardiac puncture. Plasma was separated by centrifugation for 1 min at 12,000 × *g* and stored at −20°C for further analysis. Testosterone levels in plasma were determined by established ELISA per manufacture instruction (kit #KEG010; R&D Systems).

Histology and immunohistochemical analysis. Formalin-fixed paraffin-embedded tissues were sectioned at 5-μm thickness. Tissue sections were stained with H&E (Fisher) and analyzed for cell proliferation [BrdUrd, 1:500 (BD Bioscience); Ki-67, 1:500, Clone SP6 (Lab Vision)]. The status of phospho-S6 Ribosomal Protein (1:75; Cell Signaling Technology), PTEN (1:50; Cell Signaling Technology), phospho-AKT (S473; 1:50; Cell Signaling Technology), and AR (1:150; Lab Vision) were also measured. Automated staining was done using the ChromoMap kit on the Discovery XT (Ventana Medical System, Inc.) under standard conditions. Ki67 or BrdUrd-positive cells insides the ducts (not in the stromal compartment) of entire prostate sections were counted manually and number of positive cells/ducts was calculated.

Western blotting. Tumor samples were collected, flash frozen in liquid nitrogen, and stored at −80°C until processed. Frozen samples were thawed in cold radioimmunoprecipitation assay lysis buffer [0.5 mol/L Tris-HCl (pH 7.4), 1.5 mol/L NaCl, 2.5% deoxycholic acid, 10% NP40, 10 mmol/L EDTA; Upstate USA, Inc.] containing complete protease inhibitor cocktail (Roche Diagnostics Corporation). Or tumor samples were minced and subsequently homogenized with the Qiagen bead tissue lyser. Protein concentrations in cell and tissue lysates were determined by the Bicinchoninic Acid Protein Assay kit (Pierce Biotechnology) according to the manufacturer's instructions. All proteins were detected by resolving proteins on Criterion 4-15% Tris-HCL SDS-PAGE (Bio-Rad Laboratories) and blotted onto nitrocellulose membrane. Residual binding sites were blocked by 5% nonfat dry milk and blotted with antibodies against phospho-AKT (S473; 1:1,000), phospho-S6RP (1:1,000; Cell Signaling Technology, Inc.), Amyloid Precursor Protein (1:1,000; Cell Signaling Technology, Inc.), β-Actin (1:2,000; Abcam Inc.), and Tubulin (1:1,000; Abcam Inc.). Detection of protein bands was done using SuperSignal West Pico and Femto Chemiluminescent Substrate (Pierce Biotechnology) after incubation with the horseradish peroxidase–conjugated secondary antibody (1:5,000; Jackson Immuno Research Laboratories, Inc.).

Statistical analysis. A repeated measure ANOVA followed by Dunnett's multiple comparison test was conducted to evaluate statistically significant differences of antitumor effects between groups.

Results

Detection of prostate tumors in *Pten*$^{loxP/loxP}$;C^{+} mice using noninvasive ultrasound imaging technology. For prostate tumor volume determination, we used both ultrasound and microcomputerized tomography imaging techniques (Supplementary Fig. S1). Fifty-five mice between 19 and 52 weeks of age were imaged with Ultrasound, and tumors were dissected and weighed. The smallest tumor was determined as 103 mm^3. However, we have observed that this imaging technology can detect and measure much smaller tumors (data not shown). Tumor volumes measured by three-dimensional analysis of ultrasound images correlated well with the weights of fluid-containing tumors (R^2 = 0.85; Supplementary Fig. S1). However, large tumors contained significant amounts of fluid and the volume of fluid varied markedly among tumors. Therefore, final tumor net weights showed less correlation with the ultrasound volumes at R^2 = 0.65. H&E staining confirmed

that all tumors were late stage invasive adenocarcinomas (Supplementary Fig. S1). Additionally, we were able to detect the tumor in the same mice using microcomputerized tomography (Supplementary Fig. S1); however, it was difficult to quantify the tumor volume due to the poor contrast between tumor and surrounding genitourinary organs.

Analysis of 234 *Pten*$^{loxP/loxP}$;C^{+} male mice between 20 and 76 weeks of age by ultrasound imaging showed that tumor development in this model is age dependent (Supplementary Fig. S2). All 233 animals eventually developed tumors with a minimum ultrasound volume of 12 mm^3 to a maximum of 5,410 mm^3 and one animal never developed tumor was confirmed to be misgenotyped. Tumor growth kinetics of 23 male mice over time was found to be heterogeneous (Supplementary Fig. S3). Rapidly growing tumors (16 of 23 mice) displayed doubling times of ~ 1.3 to 4.9 weeks, whereas slow growing tumors (5 of 23 mice) showed a 5.5 to 11.5 week doubling time. Two tumors seemed to be static with an extended doubling time of ~ 19 to 20 weeks.

Increased expression of phospho-Akt (S473) and phospho-S6RP in both early and late stages of tumor was associated with complete elimination of Pten expression in the luminal epithelial cells by both immunohistochemistry and Western analysis (data not shown; Supplementary Fig. S2), although other cell types remained Pten positive. Consistent with published report (32), these data suggest the PI3K pathway is activated in tumors irrespective of their age and size.

Prostate tumors in *Pten*$^{Loxp/Loxp}$;C^{+} mice are sensitive to antiandrogens. Androgen ablation has been the most common approach for late stage prostate cancer treatment in the clinic. However, hormonal deprivation therapy only remains effective for ~2 to 3 years, after which tumors develop resistance and become hormone independent. To determine androgen dependency in the Pten-deficient tumor model, 44 Pten–deficient male mice between 22 and 52 weeks of age were prescanned for enrollment. Twenty mice with tumor volumes ranging from 324 to 739 mm^3 (ages ranged from 26–46 weeks) were selected for the studies and were randomly assigned into two groups. One group was castrated by surgical removal of both testicles and the second group was assigned as controls (no surgical removal of testicles). Plasma testosterone level was measured and data showed an approximate 87% decrease upon

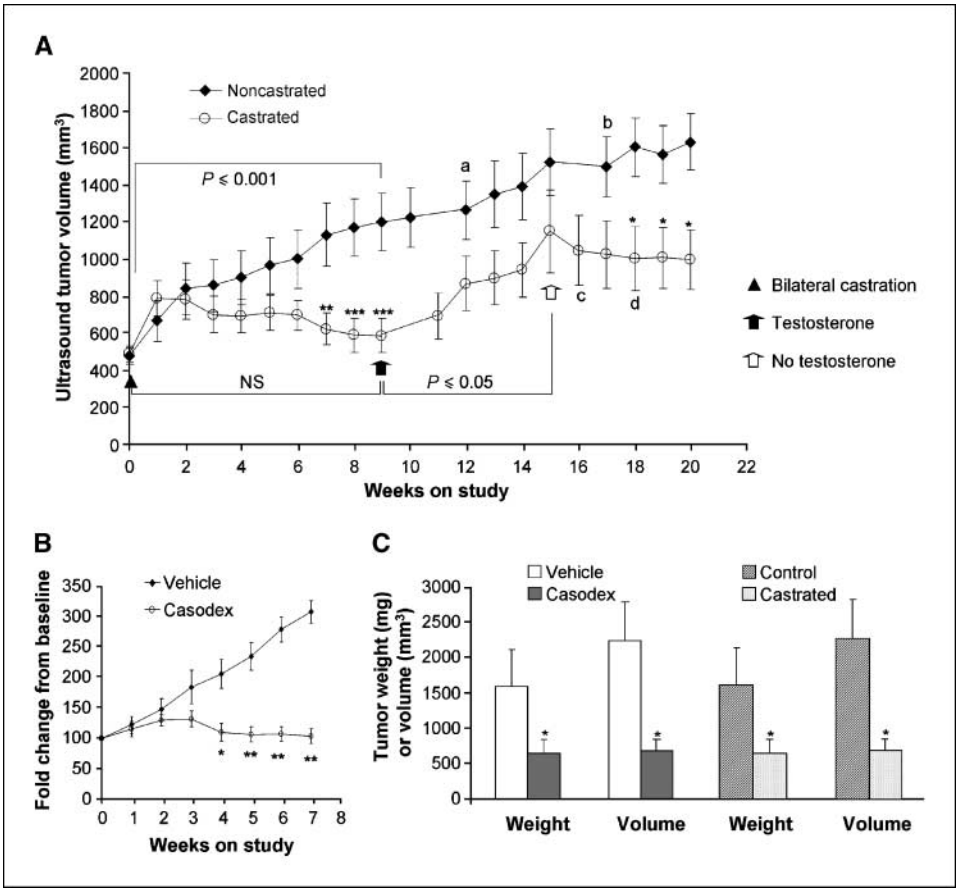

Figure 1. Pten-deficient tumors are sensitive to antiandrogens. *A,* tumor response to orchidectomy and testosterone replacement. Prostate tumors in Pten-deficient mice were imaged and the mice randomized into two groups (n = 10/group) based on tumor volume (~480 mm^3). Mice in group 1 underwent bilateral castration and those in group 2 were kept as controls. Tumors were imaged and volume was measured weekly. Testosterone pellets were implanted 9 wk following castration. Testosterone pellets were removed at the end of week 15. Few mice as indicated by *a, b, c,* and *d* (2, 4, 1, and 1, respectively) were removed from the study due to large tumor size. Tumor volume data at the time of removal was included for the duration of the study in the data analysis. Tumor growth was significantly ($P < 0.001$) different at week 9 compared with week 1 in control mice, whereas no significant (*NS*) tumor growth progression was observed between week 1 and week 9 in castrated mice. However, significant ($P < 0.05$) tumor growth progression was observed when testosterone was administered in castrated mice at week 9. *B,* mice were enrolled into two groups (n = 10/group) as per their tumor volume (~840 mm^3). Mice received either Casodex or 0.5% Methylcellulose (vehicle) and were imaged weekly. Percent change in tumor volume normalized to their baselines is depicted. Only mice that reached week 7 were included in the final data analysis. *C,* tumor weight was measured and compared with the final ultrasound measurement. *, **, and ***, statistical significances at $P < 0.05$, $P < 0.01$, and $P < 0.001$ compared with the corresponding control mice.

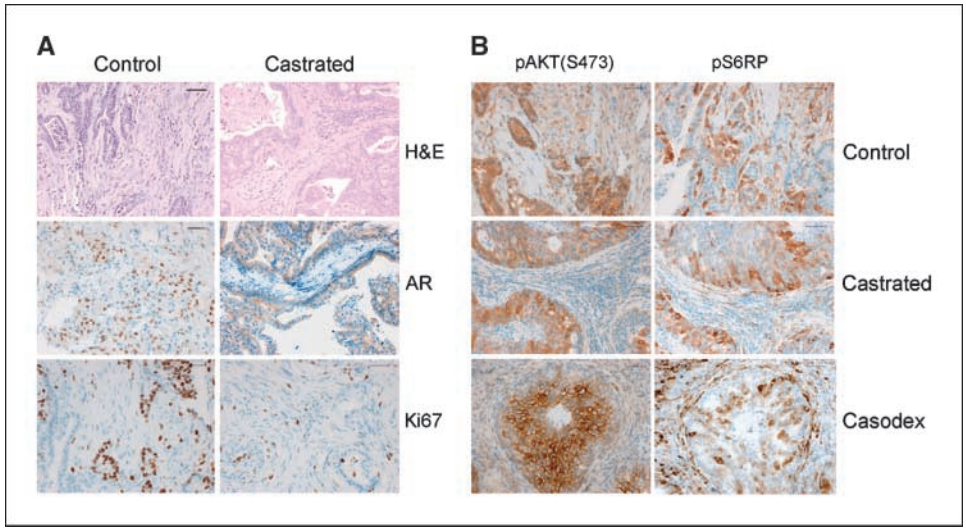

Figure 2. Androgen ablation decreases tumor cell proliferation without affecting the activation of Akt or mTOR. Tumor-bearing mice were surgically castrated or treated Casodex for 9 wk. *A,* tumor sections from noncastrated (*control*) and surgically castrated mice were stained with H&E, antibody against AR, and Ki67. *B,* tumor sections from control, surgically castrated, and Casodex-treated were stained with antibodies against pAKT(S473) and pS6RP. Representative pictures of four mice per group. *Scale bar,* 50 μm.

surgical castration compared with noncastrated control mice (Supplementary Fig. S4), which is consistent with published data (35). Mice were imaged weekly by ultrasound following enrollment into the study to monitor tumor volume. Within the first 2 weeks following surgery, we observed tumor growth in the castrated mice followed by tumor regression (Fig. 1*A*). By week 7, tumor volumes in the castrated mice were significantly smaller compared with the noncastrated controls (Fig. 1*A*). In human prostate cancer, some prostate tumors deprived of hormone-driven growth become independent and bypass the requirement for testosterone. To determine whether these tumors remained androgen sensitive, we implanted slow released (90 days) testosterone pellets (100 mg) in the surgically castrated mice at 9 weeks postsurgery. Androgen complementation resulted in tumor growth in as little as 2 weeks following testosterone implantation (Fig. 1*A*). Tumor volumes significantly increased from 586 mm^3 (week 9) to 1,147 mm^3 (week 15) after 6 weeks of testosterone treatment and no statistically significant difference was observed between the treatment and vehicle groups (Fig. 1*A*). The testosterone pellets were subsequently removed to further confirm androgen dependency of these tumors. Tumor growth was again significantly inhibited 3 weeks after the removal of testosterone pellets in castrated animals (Fig. 1*A*). Tumors were harvested and the level of androgen target was analyzed to determine the biological effects of androgens. Besides down-regulation of AR, data also showed that the level of amyloid precursor protein, another androgen target (36), was decreased (~50%) in these tumors when mice were surgically castrated (Supplementary Fig. S4; Fig. 2*A*).

To compare the effects of surgical castration to chemical castration in this model, we used the AR blocker Casodex to inhibit AR signaling. Animals with tumors ranging from 108 to 1,458 mm^3 were enrolled and treated with either vehicle (n = 9) or Casodex (n = 10) at 10 mg/kg. Due to significant tumor volumetric variations, percent change of tumor volume was used to normalize tumor growth. Additionally, as a result of unexpected animal death (not related to the toxicity of Casodex) or tumor size out of range of detection (five each group) in first 3 weeks, only mice that reached week 7 were included in the final data analysis. Data showed that Casodex (n = 5) significantly inhibits tumor growth progression (only 4% increase compared with base level), whereas in the control (n = 4), tumor volume was increased 208% (compared with the base level) in 7 weeks (Fig. 1*B*). Mice were euthanized at the end of both studies (surgical castrations and chemical castration) and tumor weight was measured. Data showed a tumor net weight reduction along with a significant reduction in ultrasound measured volume following either surgical castration or Casodex treatment (Fig. 1*C*).

Activation of Akt/mTOR pathway remained unaffected by antiandrogens treatment. Androgen blockade significantly inhibited the progression of tumor growth in this model, but did not result in a complete tumor regression. To further explore tumor signaling pathways in this model, we focused on the PI3K/Akt/mTOR signaling pathway. Published data suggests that androgen blockade increases the activation of Akt and causes androgen-refractory status in androgen-dependent prostate cancer cells (37). In contrast, Hara and colleagues (38) suggested that activated Akt is not necessary for the invasiveness of androgen-refractory MDA-I prostate cancer cells. We analyzed tumors treated with either Casodex or surgical castration by H&E and immunohistochemistry. Here, we find that residual tumors have less AR-positive cells or lower level of nuclear AR in castrated mice compared with noncastrated controls (Fig. 2*A*). Furthermore, BrdUrd labeling and Ki-67 staining of these tumors suggested that these treated tumors were less proliferative (114.82 Ki67-positive cells/duct in noncastrated prostate versus 44.06 Ki67-positive cells/duct in castrated prostate; data not shown; Fig. 2*A*). However, no significant changes in caspase activation or terminal deoxynucleotidyl transferase-mediated dUTP nick end labeling–positive cells were observed (data not shown). Adjacent tumor sections were also analyzed for changes in phospho-AKT (S473) and phospho-S6RP. Results revealed no change in the intensity of staining for either of these proteins, suggesting that both Akt and mTOR remain activated following androgen blockade by surgical castration (Fig. 2*B*). To test whether surgical and chemical castrations have different impact on the activation of Akt and mTOR, tumors treated with Casodex were stained with phospho-AKT (S473) and phospho-S6RP. Results indicated that Casodex also had no effect on the activation of Akt and mTOR in this model (Fig. 2*B*).

Combination of mTOR inhibitor and antiandrogen treatment shows additive antitumor efficacy. AR signaling and PI3K/Akt/mTOR pathways are active in a subset of human prostate cancer. Our data showed that AR and PI3K signaling pathways are

independently involved in tumor growth (Fig. 2), suggesting that simultaneously inhibition of both pathways may result in a better therapeutic response. Tumor-bearing mice were treated with either vehicle, Casodex, Rapamycin (an mTOR inhibitor), or a combination of Rapamycin and Casodex for a duration of 9 weeks. Tumors were measured once per week and tumor volumes were calculated. Significant antitumor effects of the combination group were seen as early as week 7, whereas tumor volumes of vehicle, Casodex, Rapamycin, and combination-treated mice were 1,154 + 112, 745 + 107, 637 + 128, and 417 + 129 mm^3, respectively. At 9 weeks, tumor volumes were further reduced in the combination group (411+138) compared with vehicle (1,366 + 141), Casodex (805 + 137), and Rapamycin (680 + 136) groups. Data show a significant additive antitumor effect when mice were treated with the combination of Rapamycin and Casodex (Fig. 3*A* and *B*). Mice were euthanized and tumor weights were measured at the end of the study. Tumor weight data correlated with ultrasound measurements and display an additive effect when Rapamycin was combined with Casodex (Fig. 3*C*). Similarly, combination of surgical castration and mTOR inhibitor also reduced tumor burden compared with castrated tumors (Fig. 3*D*). Together, these data suggest additive antitumor efficacy is observed when antiandrogens are combined with mTOR inhibitor. To verify that the resulting efficacy was in response to the combination, we evaluated the effect of antiandrogens and mTOR inhibitors on their respective targets by immunohistochemical analysis of tumors collected 4 hours after the last dose of the efficacy study as shown in Fig. 3*A*. Casodex alone reduced nuclear AR levels or less AR-positive cells, whereas mTOR activity remains unaffected (Fig. 4, *column 2*). Rapamycin alone completely inhibited phosphorylation of S6RP, whereas AR was not affected (Fig. 4, *column 3*). Combination treatment with Casodex and Rapamycin inhibited both AR and phospho-S6RP levels (Fig. 4, *column 4*). BrdUrd staining showed that inhibition of tumor cell proliferation by either antiandrogen or mTOR inhibitor was further enhanced by the combination (Fig. 4, *row 4*). Together, these data show that inhibition of tumor cell proliferation by blocking both pathways enhanced therapeutic efficacy.

Discussion

Application of more clinically relevant preclinical cancer models will enhance the probability of success for identification, evaluation, and development of new drug candidates for the treatment of cancer patients. Noninvasive imaging technology enable accurate

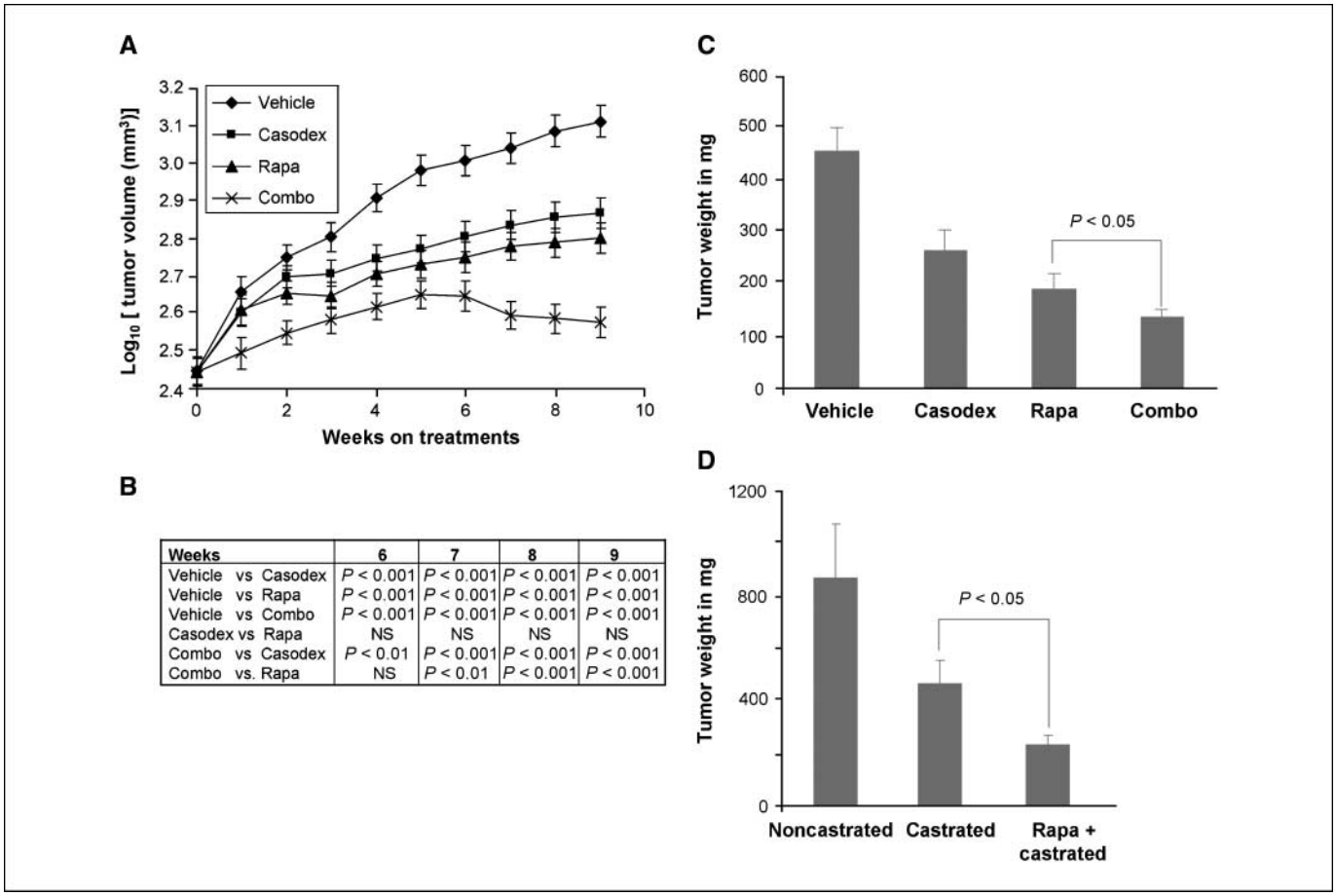

Weeks	6	7	8	9
Vehicle vs Casodex	$P < 0.001$	$P < 0.001$	$P < 0.001$	$P < 0.001$
Vehicle vs Rapa	$P < 0.001$	$P < 0.001$	$P < 0.001$	$P < 0.001$
Vehicle vs Combo	$P < 0.001$	$P < 0.001$	$P < 0.001$	$P < 0.001$
Casodex vs Rapa	NS	NS	NS	NS
Combo vs Casodex	$P < 0.01$	$P < 0.001$	$P < 0.001$	$P < 0.001$
Combo vs. Rapa	NS	$P < 0.01$	$P < 0.001$	$P < 0.001$

Figure 3. Combination of antiandrogen and mTOR inhibitor induces an additive antitumor effect. Tumor-bearing mice were enrolled when tumor size was 187 to 448 mm^3 and randomized into four groups (n = 12 mice/group). Mice were treated with either vehicle, antiandrogen (Casodex), mTOR inhibitor [Rapamycin (*rapa*)], or Casodex + Rapamycin combination for 9 wk. *A,* tumor volume was measured by ultrasound imaging. Log-transformation was applied to tumor volume for purpose of statistical analysis. Data were plotted in log scale as mean + SEM over treatment time. *B,* a repeated measure ANOVA was done to assess statistically significant differences. Between-group tests always subtract baseline group difference. *C,* mice were euthanized and tumor weight was measured and mean + SEM is plotted against treatment. *D,* in a separate study, mice with palpable tumors were surgically castrated (n = 12) and divided into two groups. Control mice (*noncastrated*; n = 6) and castrated mice (n = 6) received vehicle for 8 wk and castrated mice (n = 6) received Casodex for 8 wk. Mice were euthanized and tumor weight was measured and mean + SEM is plotted.

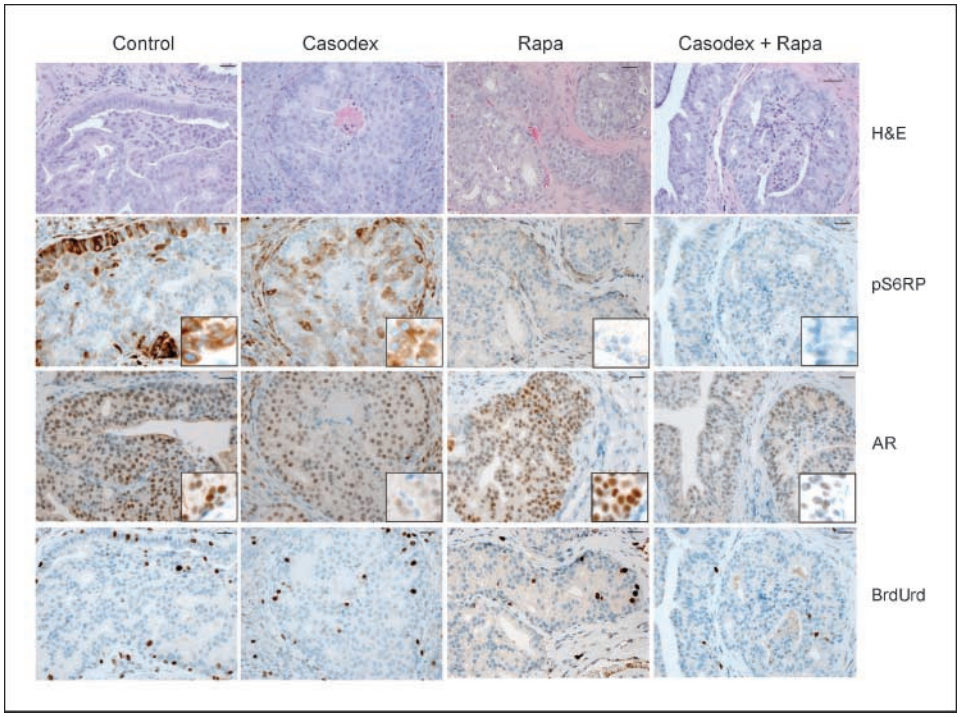

Figure 4. Inhibition of both AR and mTOR decrease tumor cell proliferation. Tumor-bearing mice were treated with vehicle (*control*), antiandrogen (Casodex), mTOR inhibitor (*Rapa*), and combination of Casodex and Rapamycin for 9 wk. Mice were euthanized and tumors were harvested 2 h after the last dose. Tumors were fixed, paraffin embedded, and sectioned. Five-micrometer-thick tumors sections were stained with H&E. Adjacent tumors sections were also stained with antibodies against phospho-S6RP (*pS6RP*), AR, or proliferation marker BrdUrd. Data represent six tumors in each treatment type. *Scale bar,* 50 μm for main images and 200 μm for insets.

quantification of tumor burden *in vivo* in real-time and facilitates the incorporation of genetically engineered mouse models in drug discovery programs. Ultrasound imaging technology was used to detect prostate tumors in the TGMAP mouse model (39, 40). However, these techniques have not been used in complex models that recapitulate human disease (such as *Pten* null mice). Here, we show that ultrasound measurements display significant correlations with actual tumor weights. We successfully show that high frequency ultrasound imaging provides a unique tool for sensitive detection of mouse prostate tumors that enables prestudy randomization based on tumor volumes and this is the first application of this imaging technique to monitor tumor progression and response to a therapy.

Tumor heterogeneity is crucial for progression, metastasis, and responsiveness to therapeutic modalities in the clinic and there are few animal models that can accurately mimic the nature of these tumors. With noninvasive imaging technologies, we have shown that following deletion of Pten, tumors in this model developed with heterogeneity and progression, which varied from tumor to tumor (Supplementary Figs. S2 and S3). Intratumor heterogeneity was also observed in this model by histologic analysis. For instance, the ratio of epithelial and stromal compartments in different sections of tumors varied and their rates of proliferation and activation of Akt or S6RP are heterogeneous, which resembles the human disease (data not shown; Supplementary Fig. S2; ref. 32).

It has been reported that early stage microscopic invasive adenocarcinoma can be detected at 16 weeks of age in the *Pten* null mouse model and they respond to castration with increasing apoptosis (32). However, residual invasive adenocarcinomas were still evident 2.5 months (10 weeks) after surgical castration (32). It has been suggested that *Pten* null prostate cancer cells can adapt to their new environment and become androgen independent (32). Our data suggest that tumors cells become less proliferative after androgen ablation compared with control but they remain sensitive to androgens (Figs. 1 and 2). When androgen was restored by implantation of testosterone pellets in the surgically castrated mice, the tumor growth progression resumed at a similar rate as the control animals (Fig. 1*A*). However, it is possible that 9 weeks of androgen ablation was insufficient to deplete the entire population of androgen dependent tumor cells and the remaining androgen-dependent tumor cells were still sensitive to testosterone (Fig. 1*A*).

The molecular mechanism underlying the initiation of androgen refractory prostate cancer is relatively unknown. PI3K/AKT/mTOR signaling pathways play a major role in the initiation and progression of these tumors in many preclinical mouse models, and cell-based data suggest that the PI3K/AKT/mTOR signaling network is also responsible for the development of androgen refractory tumors. However, this hypothesis has not been tested in any relevant preclinical models. Here, we show that *Pten* null prostate tumors are sensitive to antiandrogen treatment and remain androgen dependent without affecting the activation of Akt and mTOR (Fig. 2*B*). However, it might be possible for some tumors to escape after long-term treatment with antiandrogens in this model. These data suggest that the activation of the Akt or mTOR signaling network may not be the sole factor driving the development of an androgen refractory state when treated with antiandrogens.

Antiandrogens or complete androgen blockade and conventional chemotherapeutic approaches are effective in androgen-dependent prostate cancer (41). However, these agents do not result in complete tumor regression and clearance. Similarly, it has been shown that mTOR inhibitors reverse Pten/Akt/mTOR-mediated neoplasia and reduce tumor volumes in engineered mice (12, 13, 42). More recently, Kinkade and colleagues (43) and Carracedo and colleagues (44) reported that the combination of PI3K pathway inhibitor with extracellular signal-regulated kinase/mitogen-activated protein kinase signaling inhibitor might be more useful in preclinical models of hormone refractory prostate

cancer. We have shown that combination of a PI3K pathway inhibitor with antiandrogen shows an additive benefit compared with any single agent alone in this mouse model of prostate cancer (Fig. 3). Our data indicate a rationale for combinational strategies of androgen blockade with either Akt and/or mTOR inhibition for further exploration in clinic.

In summary, high frequency ultrasound imaging is a very useful technique to randomize and monitor tumor growth progression of prostate cancer in the *Pten*$^{loxP/loxP}$;C^{+} model. Ultrasound as a method of tracking tumor progression enables a generalized application of these techniques in genetic mouse models for evaluation of preclinical drug candidates. The *Pten* null prostate tumor model resembles androgen-dependent prostate cancer in patients and responds to complete androgen blockade. In addition, activation of the Akt and mTOR pathway remained unchanged after chronic treatment with antiandrogens and combinations of antiandrogen and PI3K pathway inhibitor enhanced the efficacy of antiandrogens.

Disclosure of Potential Conflicts of Interest

All authors are or were employed by Merck & Co., Inc.

Acknowledgments

Received 11/17/08; revised 6/24/09; accepted 7/12/09; published OnlineFirst 9/8/09.

The costs of publication of this article were defrayed in part by the payment of page charges. This article must therefore be hereby marked *advertisement* in accordance with 18 U.S.C. Section 1734 solely to indicate this fact.

We thank Nirah Shomer, Merck Research Laboratories-Boston, for providing animal resource support; Matthew III Walker for use of ultrasound imaging system; Christopher Tong and Shubing Wang, Merck Research Laboratories-West Point, for statistical analysis; and Katharine Ellwood-Yen, Merck Research Laboratories-Boston, for her critical comments in this manuscript.

References

1. Baade PD, Coory MD, Aitken JF. International trends in prostate-cancer mortality: the decrease is continuing and spreading. Cancer Causes Control 2004;15:237–41.
2. Ricke WA, Wang Y, Cunha GR. Steroid hormones and carcinogenesis of the prostate: the role of estrogens. Differentiation 2007;75:871–82.
3. Michaelson MD, Cotter SE, Gargollo PC, Zietman AL, Dahl DM, Smith MR. Management of complications of prostate cancer treatment. CA Cancer J Clin 2008;58:196–213.
4. Bolla M, Gonzalez D, Warde P, et al. Improved survival in patients with locally advanced prostate cancer treated with radiotherapy and goserelin. N Engl J Med 1997;337:295–300.
5. Lu-Yao GL, Albertsen PC, Moore DF, et al. Survival following primary androgen deprivation therapy among men with localized prostate cancer. JAMA 2008;300:173–81.
6. Pomerantz M, Kantoff P. Advances in the treatment of prostate cancer. Annu Rev Med 2007;58:205–20.
7. Xu Y, Chen SY, Ross KN, Balk SP. Androgens induce prostate cancer cell proliferation through mammalian target of Rapamycin activation and post-transcriptional increases in cyclin D proteins. Cancer Res 2006;66:7783–92.
8. Sun M, Yang L, Feldman RI, et al. Activation of phosphatidylinositol 3-kinase/Akt pathway by androgen through interaction of p85α, androgen receptor, and Src. J Biol Chem 2003;278:42992–3000.
9. Baron S, Manin M, Beaudoin C, et al. Androgen receptor mediates non-genomic activation of phosphatidylinositol 3-OH kinase in androgen-sensitive epithelial cells. J Biol Chem 2004;279:14579–86.
10. Myers MP, Stolarov JP, Eng C, et al. P-TEN, the tumor suppressor from human chromosome 10q23, is a dual-specificity phosphatase. Proc Natl Acad Sci U S A 1997; 94:9052–7.
11. Aoki M, Batista O, Bellacosa A, Tsichlis P, Vogt PK. The akt kinase: molecular determinants of oncogenicity. Proc Natl Acad Sci U S A 1998;95:14950–5.
12. Neshat MS, Mellinghoff IK, Tran C, et al. Enhanced sensitivity of PTEN-deficient tumors to inhibition of FRAP/mTOR. Proc Natl Acad Sci U S A 2001;98:10314–9.
13. Podsypanina K, Lee RT, Politis C, et al. An inhibitor of mTOR reduces neoplasia and normalizes p70/S6 kinase activity in Pten+/− mice. Proc Natl Acad Sci U S A 2001; 98:10320–5.
14. Stiles B, Gilman V, Khanzenzon N, et al. Essential role of AKT-1/protein kinase B α in PTEN-controlled tumorigenesis. Mol Cell Biol 2002;22:3842–51.
15. Gray IC, Phillips SM, Lee SJ, Neoptolemos JP, Weissenbach J, Spurr NK. Loss of the chromosomal region 10q23–25 in prostate cancer. Cancer Res 1995;55: 4800–3.
16. Komiya A, Suzuki H, Ueda T, et al. Allelic losses at loci on chromosome 10 are associated with metastasis and progression of human prostate cancer. Genes Chromosomes Cancer 1996;17:245–53.
17. Li J, Yen C, Liaw D, et al. PTEN, a putative protein tyrosine phosphatase gene mutated in human brain, breast, and prostate cancer. Science 1997;275:1943–7.
18. Li DM, Sun H. TEP1, encoded by a candidate tumor suppressor locus, is a novel protein tyrosine phosphatase regulated by transforming growth factor β. Cancer Res 1997;57:2124–9.
19. Steck PA, Pershouse MA, Jasser SA, et al. Identification of a candidate tumour suppressor gene, MMAC1, at chromosome 10q23.3 that is mutated in multiple advanced cancers. Nat Genet 1997;15:356–62.
20. Dong JT, Isaacs WB, Isaacs JT. Molecular advances in prostate cancer. Curr Opin Oncol 1997;9:101–7.
21. Gray IC, Stewart LM, Phillips SM, et al. Mutation and expression analysis of the putative prostate tumour-suppressor gene PTEN. Br J Cancer 1998;78:1296–300.
22. Wang SI, Parsons R, Ittmann M. Homozygous deletion of the PTEN tumor suppressor gene in a subset of prostate adenocarcinomas. Clin Cancer Res 1998;4:811–5.
23. Suzuki H, Freije D, Nusskern DR, et al. Interfocal heterogeneity of PTEN/MMAC1 gene alterations in multiple metastatic prostate cancer tissues. Cancer Res 1998;58:204–9.
24. Vlietstra RJ, van Alewijk DC, Hermans KG, van Steenbrugge GJ, Trapman J. Frequent inactivation of PTEN in prostate cancer cell lines and xenografts. Cancer Res 1998;58:2720–3.
25. Di Cristofano A, Pesce B, Cordon-Cardo C, Pandolfi PP. Pten is essential for embryonic development and tumour suppression. Nat Genet 1998;19:348–55.
26. Podsypanina K, Ellenson LH, Nemes A, et al. Mutation of Pten/Mmac1 in mice causes neoplasia in multiple organ systems. Proc Natl Acad Sci U S A 1999; 96:1563–8.
27. Majumder PK, Sellers WR. Akt-regulated pathways in prostate cancer. Oncogene 2005;24:7465–74.
28. Engelman JA, Luo J, Cantley LC. The evolution of phosphatidylinositol 3-kinases as regulators of growth and metabolism. Nat Rev Genet 2006;7:606–19.
29. Vivanco I, Sawyers CL. The phosphatidylinositol 3-Kinase AKT pathway in human cancer. Nat Rev Cancer 2002;2:489–501.
30. Majumder PK, Yeh JJ, George DJ, et al. Prostate intraepithelial neoplasia induced by prostate restricted Akt activation: the MPAKT model. Proc Natl Acad Sci U S A 2003;100:7841–6.
31. Majumder PK, Grisanzio C, O'Connell F, et al. A prostatic intraepithelial neoplasia-dependent p27 Kip1 checkpoint induces senescence and inhibits cell proliferation and cancer progression. Cancer Cell 2008;14:146–55.
32. Wang S, Gao J, Lei Q, et al. Prostate-specific deletion of the murine Pten tumor suppressor gene leads to metastatic prostate cancer. Cancer Cell 2003;4:209–21.
33. Lesche R, Groszer M, Gao J, et al. Cre/loxP-mediated inactivation of the murine Pten tumor suppressor gene. Genesis 2002;32:148–9.
34. Wu X, Wu J, Huang J, et al. Generation of a prostate epithelial cell-specific Cre transgenic mouse model for tissue-specific gene ablation. Mech Dev 2001;101:61–9.
35. Hunag B, Leu S, Yang H, Norman R. Testosterone effects on luteinizing hormone and follicle-stimulating hormone responses to gonadotropin-releasing hormone in the mouse. J Androl 2001;22:507–13.
36. Takayama K, Tsutsumi S, Suzuki T, et al. Amyloid precursor protein is a primary androgen target gene that promotes prostate cancer growth. Cancer Res 2009;69:137–42.
37. Murillo H, Huang H, Schmidt LJ, Smith DI, Tindall DJ. Role of PI3K signaling in survival and progression of LNCaP prostate cancer cells to the androgen refractory state. Endocrinology 2001;142:4795–805.
38. Hara T, Miyazaki H, Lee A, Tran CP, Reiter RE. Androgen receptor and invasion in prostate cancer. Cancer Res 2008;68:1128–35.
39. Wu G, Wang L, Yu L, Wang H, Xuan JW. The use of three-dimensional ultrasound micro-imaging to monitor prostate tumor development in a transgenic prostate cancer mouse model. Tohoku J Exp Med 2005;207:181–9.
40. Wirtzfeld LA, Wu G, Bygrave M, et al. A new three-dimensional ultrasound microimaging technology for preclinical studies using a transgenic prostate cancer mouse model. Cancer Res 2005;65:6337–45.
41. Pienta KJ, Smith DC. Advances in prostate cancer chemotherapy: a new era begins. CA Cancer J Clin 2005; 55:300–18; quiz 23–5.
42. Majumder PK, Febbo PG, Bikoff R, et al. mTOR inhibition reverses Akt-dependent prostate intraepithelial neoplasia through regulation of apoptotic and HIF-1-dependent pathways. Nat Med 2004;10: 594–601.
43. Kinkade CW, Castillo-Martin M, Puzio-Kuter A, et al. Targeting AKT/mTOR and ERK MAPK signaling inhibits hormone-refractory prostate cancer in a preclinical mouse model. J Clin Invest 2008; 118:3051–64.
44. Carracedo A, Ma L, Teruya-Feldstein J, et al. Inhibition of mTORC1 leads to MAPK pathway activation through a PI3K-dependent feedback loop in human cancer. J Clin Invest 2008;118:3065–74.